

REPORT DOCUMENTATION PAGE

Form Approved
OMB No. 0704-0188

Public reporting burden for this collection of information is estimated to average 1 hour per response, including the time for reviewing instructions, searching existing data sources, gathering and maintaining the data needed, and completing and reviewing this collection of information. Send comments regarding this burden estimate or any other aspect of this collection of information, including suggestions for reducing this burden to Department of Defense, Washington Headquarters Services, Directorate for Information Operations and Reports (0704-0188), 1215 Jefferson Davis Highway, Suite 1204, Arlington, VA 22202-4302. Respondents should be aware that notwithstanding any other provision of law, no person shall be subject to any penalty for failing to comply with a collection of information if it does not display a currently valid OMB control number. **PLEASE DO NOT RETURN YOUR FORM TO THE ABOVE ADDRESS.**

1. REPORT DATE (DD-MM-YYYY) 05-09-2005		2. REPORT TYPE REPRINT		3. DATES COVERED (From - To)	
4. TITLE AND SUBTITLE Thermospheric Infrared Radiance Response to the April 2002 Geomagnetic Storm from SABER Infrared and GUVI Ultraviolet Limb Data				5a. CONTRACT NUMBER	
				5b. GRANT NUMBER	
				5c. PROGRAM ELEMENT NUMBER 62601F	
6. AUTHOR(S) Jeremy R. Winick ¹ , M.G. Mlynczak ² , P.P. Wintersteiner ³ , F.-J. Martin-Torres ⁴ , R.H. Picard ¹ , L. Paxton ⁵ , M. Lopez-Puerta ⁶ , J.M. Russell ⁷ , A. Christensen ⁸ , and L. Gordley ⁹				5d. PROJECT NUMBER 2301	
				5e. TASK NUMBER BD	
				5f. WORK UNIT NUMBER A1	
7. PERFORMING ORGANIZATION NAME(S) AND ADDRESS(ES) Air Force Research Laboratory 29 Randolph Road Hanscom AFB, MA 01731-3010				8. PERFORMING ORGANIZATION REPORT NUMBER AFRL-VS-HA-TR-2005-1098	
9. SPONSORING / MONITORING AGENCY NAME(S) AND ADDRESS(ES)				10. SPONSOR/MONITOR'S ACRONYM(S) AFRL/VSBYB	
				11. SPONSOR/MONITOR'S REPORT NUMBER(S)	
12. DISTRIBUTION / AVAILABILITY STATEMENT Approved for Public Release; Distribution Unlimited.					
<p>¹Air Force Research Laboratory, Space Vehicles Directorate; ²NASA Langley Research Center; ³ARCON Corp.; ⁴A S & M Corp.; ⁵John Hopkins University/Applied Physics Laboratory; ⁶Instituto de Astrofisica de Andalucia; ⁷Hampton University; ⁸Aerospace Corp.; ⁹GATS, Inc.</p>					
13. SUPPLEMENTARY NOTES Reprinted from: Remote Sensing of Clouds and the Atmosphere VIII, Proceedings of SPIE Vol. 5235 (SPIE, Bellingham, WA2004), Pages 250 - 263					
14. ABSTRACT The SABER instrument on TIMED continuously measures certain infrared limb radiance profiles with unprecedented sensitivity. Among these are emissions of CO ₂ v ₃ at 4.3 μm, routinely recorded to tangent heights of ~140-150 km, and NO at 5.3 μm, seen to above 200 km. Both of these are greatly enhanced during periods of strong auroral activity, when they can be measured to ~200 km and ~300 km, respectively. We use these infrared channels of SABER and coincident far ultraviolet (FUV) measurements from GUVI on TIMED, to study the geomagnetic storm of April 2002. These all give a consistent measure of auroral energy input into the lower thermosphere at high latitudes. Emission in yet another SABER channel, near 2.0 μm, correlates well with enhanced electron energy deposition. We also have, in the 5.3-μm emissions from the long-lived population of aurorally produced NO, a tracer of how this energy is transported equator-ward and released over an extended period of time, a few days. In this paper, we discuss the global patterns of energy deposition into the expanded auroral oval, its transport to lower latitudes, and its loss as revealed by the NO 5.3-μm emissions.					
15. SUBJECT TERMS Aurora, Infrared radiance, Thermosphere, Infrared cooling CO ₂ , NO, Atmospheric heating					
16. SECURITY CLASSIFICATION OF:			17. LIMITATION OF ABSTRACT SAR	18. NUMBER OF PAGES 14	19a. NAME OF RESPONSIBLE PERSON Richard H. Picard
a. REPORT UNCLAS	b. ABSTRACT UNCLAS	c. THIS PAGE UNCLAS			19b. TELEPHONE NUMBER (include area code) 781-377-2222

Thermospheric infrared radiance response to the April 2002 geomagnetic storm from SABER infrared and GUVI ultraviolet limb data

Jeremy R. Winick^a, M.G. Mlynczak^b, P.P. Wintersteiner^c, F.-J. Martin-Torres^d, R.H. Picard^a, L. Paxton^e, M. Lopez-Puertas^f, J.M. Russell^g, A. Christensen^h, and L. Gordleyⁱ

^aAir Force Research Laboratory, Space Vehicles Directorate; ^bNASA Langley Research Center; ^cARCON Corp.; ^dA S & M Corp; ^eJohns Hopkins University/Applied Physics Laboratory; ^fInstituto de Astrofísica de Andalucía; ^gHampton University; ^hAerospace Corp.; ⁱGATS, Inc.

ABSTRACT

The SABER instrument on TIMED continuously measures certain infrared limb radiance profiles with unprecedented sensitivity. Among these are emissions of CO₂ v₃ at 4.3 μm, routinely recorded to tangent heights of ~140-150 km, and NO at 5.3 μm, seen to above 200 km. Both of these are greatly enhanced during periods of strong auroral activity, when they can be measured to ~200 km and ~300 km, respectively. We use these infrared channels of SABER and coincident far ultraviolet (FUV) measurements from GUVI on TIMED, to study the geomagnetic storm of April 2002. These all give a consistent measure of auroral energy input into the lower thermosphere at high latitudes. Emission in yet another SABER channel, near 2.0 μm, correlates well with enhanced electron energy deposition. We also have, in the 5.3-μm emissions from the long-lived population of aurorally produced NO, a tracer of how this energy is transported equatorward and released over an extended period of time, a few days. In this paper, we discuss the global patterns of energy deposition into the expanded auroral oval, its transport to lower latitudes, and its loss as revealed by the NO 5.3-μm emissions.

Keywords: Aurora, CO₂, NO, Infrared radiance, Thermosphere, Atmospheric heating, Infrared cooling

1. INTRODUCTION

Geomagnetic storms are one of the clearest manifestations of Sun-Earth coupling. During such storms, vivid auroral displays often occur at lower latitudes where they are otherwise rare events. This increased auroral activity along with increased Joule heating is believed to increase rapidly the temperature of the upper atmosphere and produce other dynamical and chemical perturbations. The TIMED¹ spacecraft is a major force in NASA's Sun-Earth-Connection program to examine how solar conditions impact the earth environment. TIMED is uniquely designed to study the changes in the earth's mesosphere and lower thermosphere (60-180km) on a nearly continuous global scale. Using the data from the SABER (Sounding of the Atmosphere using Broadband Emission Radiometry) instrument we examine the global inflow and outflow of energy as sensed during the April 2002 geomagnetic storm. The energy inflow is sensed from the GUVI (Global Ultraviolet Imager) LBH-2 band and the SABER infrared 4.3-μm band, as well as the 2.0-μm band that records an unknown aurorally sensitive species. The outflow is measured using the SABER 5.3-μm band.

2. TIMED SPACECRAFT

TIMED¹ was launched on Dec. 7, 2001 into a circular 625km orbit with a declination of 74 degrees, outfitted with four experiments: SABER, GUVI, SEE and TIDI. These make global measurements of the 60-180km altitude region, long

* <mailto:jeremy.winick@hanscom.af.mil>; phone +01-781-377-3619; fax 01-781-377-8900; Air Force Research Laboratory, Space Vehicles Dir., 29 Randolph Road, Hanscom AFB, MA 01731-3010, USA

DISTRIBUTION STATEMENT A

Approved for Public Release
Distribution Unlimited

called the "ignorosphere" because of the lack of direct measurements there. This region is difficult to explore with *in situ* probes because it is above balloon altitudes and below stable satellite orbits. Previous data have come either from sounding rockets, necessarily isolated in space and time, or ground-based remote sensing, which is also limited in spatial coverage. We will use data from SABER and GUVI for this paper.

2.1 SABER

SABER² is a ten-channel radiometer that scans the limb scans up to almost 350km tangent height using a moving mirror. Radiance data are spaced every 0.4km in tangent height within a ~2km FOV, so the data are oversampled. The focal plane set-up is shown in Figure 1. We will primarily use data from channels 6 (NO 5.3 μm) and 7 (CO₂ 4.3 μm and NO⁺) but also present data from channel 8 (2.0 μm). The filters are such that most, but not all of these emissions fall within the respective bandpasses.

The limb-viewing SABER instrument must always look away from the sun. This requires that a yaw maneuver be performed about every 60 days. Since the instrument is looking perpendicular to the satellite track out the cold side of the spacecraft, the range of latitudes covered at the tangent point varies with the phase of the yaw cycle, alternating between 53S-83N and 83S-53N. Thus high latitudes are fully accessible in only one hemisphere at a time. Moreover, the orbit precesses slowly, allowing a large range of local times to be sampled at any given latitude during each yaw cycle. During the April 2002 storm, SABER was looking south, and local times were such that virtually all measurements were made in darkness, enabling the continual observation of aurora.

2.2 GUVI

GUVI³ is a FUV spectral imager that has spatial and spectral pixels. GUVI images both the limb and below the horizon (earth-disk). It uses a moving mirror to scan a 140-degree swath in the cross-track direction from 520km tangent height in the limb on the dark side of the spacecraft (the same side as SABER views the limb) down through nadir and beyond. The focal plane array is made up of 14 spatial pixels along the orbit track direction and spectral pixels across track. We use the limb data, picking image pixels as close as possible to the SABER line-of-sight (LOS) tangent points. Note that there are about 400 GUVI swaths per orbit and only about 100 SABER limb scans. This faster scan rate, along with the 14 spatial pixels, provides a much higher density of horizontal measurements in GUVI. But GUVI's limb tangent heights, about 18 km apart, are spaced much more sparsely than SABER's. We use Lyman-Birge-Hopfield emissions (the GUVI LBH2 band, 165-180nm) for our analysis.

3. ENERGY INPUT—IR AND UV INDICATORS

3.1 Infrared Aurora

Auroral enhancements in the infrared have been known since the 1970's^{4,5,6}. The most prominent emissions are in CO₂ at 4.3 μm, NO at the 5.3-μm rovibrational fundamental and the 2.7-μm overtone, and NO⁺ at 4.3 μm⁷. The 4.3-μm and 5.3-μm bands are measured in SABER channels 7 and 6, respectively (Figure 1). Both of these channels detect significant emission under quiescent conditions^{8,9,10} and are enhanced by chemical and vibrational energy transfer processes during aurora. The CO₂ 4.3-μm emission during aurora comes primarily from the CO₂ v₃ (00011) state^{7,11} (HITRAN notation), excited by V-V transfer collisions with N₂(v=1),



following electron excitation or chemical excitation of N₂(v):



In the quiescent nighttime atmosphere, reactions 2-4 essentially disappear and the CO₂ (00011) population is quite low. In that case, in the mesosphere it is maintained by collision with N₂(v), via reaction 1, by collisions which interchange CO₂ v₃ with multiple CO₂ v₂ quanta^{8,10}, and by radiative transfer from the stratopause region. Above the mesopause, radiative transfer effects become dominant. In the daytime, very efficient solar excitation of CO₂ at 4.3 μm and in hot bands at 2.7 and 2.0 μm, leads to large non-LTE enhancements. This greatly enhances the radiance starting as low as 50-60km, and masks all but the strongest auroras for altitudes above 100km. For these reasons we restrict our analysis to nighttime conditions for solar zenith angle (SZA) >105°. As noted in Section 2.1, during the period April 10-25 the orbit was such that this criterion was satisfied most of the time, giving maximum coverage for auroral observations.

NO⁺(v) is excited primarily by the ion-molecule reactions



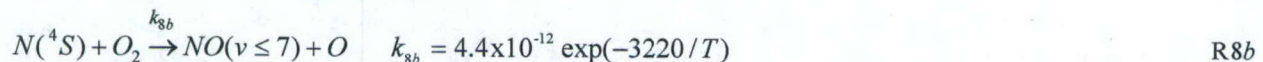
The vibrational distribution in the product NO⁺ has been measured in the laboratory for reaction 5 by *Smith et al*¹², but for reaction 6 one had to estimate the vibrational yield in order to model auroral data⁷.

The CO₂ mechanism requires the transfer of N₂(v) quanta to CO₂ v₃, a process that takes minutes at 90km and tens of minutes or more at altitudes above 100km. Moreover, the CO₂ emission is optically thick in the limb for the major isotope (¹⁶O¹²C¹⁶O) fundamental at altitudes below about 110km. The NO⁺ emission, however, although severely quenched below 110km, is prompt (lifetime seconds or less due to the fast ion-molecule reactions R5-R6) and optically thin⁷. These complications make the modeling of auroral 4.3-μm limb radiance notoriously difficult. In particular, the auroral dosing must be known along the line-of-sight and at previous times. The mixture of prompt NO⁺ and non-prompt CO₂ emissions can therefore not be determined without either very high resolution spectra or pre-dosing and spatial information which are not available for SABER. Thus the 4.3-μm enhancement is a good indication of auroral activity, but we cannot expect it to exactly correlate with an entirely prompt emission such as LBH, in space or time.

NO(v=1) is excited by V-T collisions with ambient atomic oxygen by the reverse of the exothermic reaction



for which a recent measurement¹³ yielded $k_7 = 4.2 \times 10^{-11} \text{ cm}^3 \text{ s}^{-1}$. Excitation is very temperature sensitive because of the $\exp(-2698/T)$ factor arising from detailed balance. This reaction, in combination with the emission at 5.3 μm¹⁴ that is observed by SABER, is responsible for NO being the principal cooling agent for the thermosphere between ~120 and 200 km¹⁵. Chemical reactions¹⁶⁻¹⁹ also produce NO(v>0), preferably populating v>1:



Atomic nitrogen in either the ground state (⁴S) or excited state (²D) is produced copiously in aurora, but k_{8a} is much faster than k_{8b} due to the large activation energy of the latter (about 0.3eV or 3220 K). However, the fact that reaction 8b becomes more efficient at higher temperatures does affect the NO emission, especially after the atmosphere has been heated by geomagnetic storm effects. During the April 2002 storm there was a quieter day on April 21 before the last disturbed days on April 22-23 where this effect can be seen.

3.2 FUV Emission

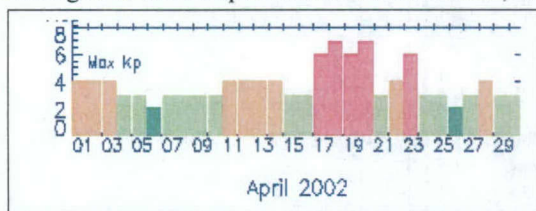
Electron impact excitation is the principal cause of the emissions of molecular nitrogen. In particular, the Lyman-Birge-Hopfield (LBH) system, a ¹Π_g → X¹Σ_g⁺, which is electric-dipole forbidden, is excited by photoelectrons in the daytime, and by auroral secondaries and degraded primaries^{20,21}. Even so, the radiative lifetime is short enough (80 μsec) that quenching is not important in the lower thermosphere. LBH is therefore a good monitor of auroral dosing strength.

However, atmospheric absorption, including self-absorption and absorption in the O₂ Schumann-Runge continuum (SRC), can be a problem for limb observations in the lower thermosphere.

LBH bands are found between ~125 and 200 nm, and the GUVI spectral range is 115-180 nm. Of the two LBH data products that are provided, we chose the longer-wavelength one (LBH-2, 165-180 nm) as an indicator of auroral energy input, because of the much-reduced effect of absorption at the long end of the SRC, ~175 nm. We estimate that at 125 km tangent height, LBH self-absorption is small. The GUVI/SABER coincidences of most interest are at tangent heights of ~115-130 km.

3.3 Storm Activity

A series of coronal mass ejections occurred on the Sun near the middle of April 2002, with energetic particle streams arriving at Earth on April 17 and 19. As a result, strong magnetic storms persisted for several days, reaching their peak on April 20. Geomagnetic activity is summarized in the adjoining chart, which shows the daily Kp for the entire month. Activity is relatively low through April 10. Then a slight rise is seen between April 11 and April 14, followed by another brief quiescent period before the storm hit on the 17th. A subsequent burst of activity on the 23rd was the result of a solar flare two days earlier.



As shown below, several of the infrared emissions detected by SABER were strongly affected by this magnetic activity. Pre-storm nighttime emissions from April 10-15 are used as a baseline for comparison with the greatly-enhanced levels of subsequent days.

As shown below, several of the infrared emissions detected by SABER were strongly affected by this magnetic activity. Pre-storm nighttime emissions from April 10-15 are used as a baseline for comparison with the greatly-enhanced levels of subsequent days.

3.4 Channel 7 Radiance

The global morphology of SABER channel-7 limb (4.3- μ m) emission at 120km tangent altitude is shown for four storm days, April 17-20, in Figure 2. The large enhancements appear to be restricted to the auroral zones. The northern auroral zone is largely not seen due to the viewing geometry mentioned above. It should be noted that the global maps are made from limb radiances measured in the fifteen orbits for each day and thus are not snapshots. The horizontal structure is caused by the time dependence of the energy input and the displacement of the geomagnetic coordinate system from the geographic. Since the nighttime excitation mechanisms for the 4.3 μ m emission are largely absent, except for auroral excitation by reactions 2-6, and enhanced N₂(v) can be transported at most a few hundred kilometers during its lifetime, the observed restriction to the auroral zone is expected. This can be seen more clearly in Figure 3, where we plot all channel 7 nighttime radiance levels (SZA>105°) at a tangent height of 110km as a function of magnetic latitude for a quiet day and a storm day. On April 10, a very quiet day, there was little difference between radiance in the auroral zone and that at lower latitudes. By April 15 (not shown) there were a few modest enhancements over a narrow range of very high latitudes. On storm days, such as April 18, increases of more than a factor of ten appeared over a much wider range of magnetic latitude. On these days, the radiance levels of virtually all events in the core of the auroral zone were greater than those seen on April 10.

Figure 4 shows individual and composite radiance profiles from channel 7, to illustrate the event-to-event variability and the complicated nature of the auroral scans. Here, we contrast the daily mean profile for quiet events in the latitude bin 30-50N for April 18, shown with the rms deviation from the mean, with four separate events within the extended auroral zone. Quiet events were those having radiance levels in the lower thermosphere comparable to low-latitude norms. The four consecutive events showing indications of auroral activity, one of them with radiance increased by a factor of twenty, had tangent points between 50 and 44N. The fact that enhancements appear down to 60 km in three of them indicates that the dosing regions were closer to the satellite than the tangent point, consistent with the fact that SABER was looking roughly southward at the time. The 4.3- μ m bands are optically very thick, so near-side auroras usually appear to be more intense. Also, as mentioned earlier, the CO₂ signal is not prompt with respect to the dosing. In fact, the radiance at a given tangent height depends in a very complicated way on the location, intensity, and timing of the auroral dosing and also upon the way the instrument LOS cuts through the affected region. It follows that assigning an auroral event location to the tangent point can be somewhat misleading. In this case, it may suggest a larger expansion of the auroral zone than is actually warranted.



3.5 Comparison with GUVI and SABER Channel 8 (2.1 μm)

Figure 5 shows a storm-day correlation between the SABER channel-7 radiance at 120km and the GUVI LBH-2 band intensities for the lowest limb path available, $\sim 130\text{km}$. To make the comparison, for each SABER event we selected the GUVI event nearest in time and the GUVI spatial pixels that were in closest coincidence with the SABER tangent point. Note that GUVI has a significantly lower dynamic range than SABER. There is no significant nighttime excitation for LBH outside the auroral zone, and radiance levels are in the noise, which accounts for the paucity of points there. Nevertheless, the prompt LBH and the somewhat-delayed CO_2 emissions clearly have the same global morphology, indicating that the infrared source is an excellent qualitative indicator of auroral dosing intensity.

Channel 8 on SABER with a bandpass of $\sim 1.95\text{-}2.2 \mu\text{m}$ is designed to measure the $\Delta v=2$ OH Meinel emission from the high vibration levels ($v=9, 8, 7$) of OH(v). The source of the excited OH is the reaction,



SABER normally observes the OH(v) emission falling off rapidly above its peak at around 87 km and merging with the noise level by 105km. This behavior is to be expected since the O_3 reactant in reaction 9 falls off rapidly with altitude above the peak. It is formed by a three-body reaction, $\text{O} + \text{O}_2 + \text{M}$, where M is any third body, and thus its rate of formation is proportional to the square of the exponentially decreasing background density. Nevertheless, there is a clear auroral signal in this channel. For quiescent nighttime events, including all low-latitude events, the radiance above 100 km is at the instrument noise level. But for events where GUVI and SABER channel 7 detect enhanced emissions, channel 8 is also elevated, with radiance levels on the order of $10^{-9} \text{ W/cm}^2\text{-sr}$ at 120 km and quite a slow falloff with tangent height. The source of the channel-8 emissions is uncertain at the present time, but its association with the aurora is clear. A global map of channel-8 radiance, for lower-thermospheric tangent heights on storm days (not shown), has patterns that are quite similar to those in Figure 5. Even more specifically, the event-by-event intensity levels in the auroral zone correlate very strongly with those of channel 7 and GUVI LBH-2.

The latter point is illustrated in Figure 6, where we compare radiance levels from both channels 7 and 8 with GUVI, for all events poleward of 50 degrees magnetic latitude on a typical storm day. The CO_2 emission correlates broadly with LBH, but the plot does show many events with elevated FUV accompanied by rather weak $4.3\text{-}\mu\text{m}$ intensities. This is expected, because the opacity of the atmosphere reduces the CO_2 signal for distant auroras, and for other reasons mentioned in the previous section. Also expected is the offset from the origin, due to normal (quiescent) nighttime CO_2 radiance levels. The channel-8 signal, however, correlates much more completely with GUVI, showing a clear linear trend and no offset. On this basis, the channel-8 emission appears to be completely of auroral origin, prompt, and optically thin in the limb. To strengthen this point, we note that no correlation exists among any of these radiance levels for non-storm days or low-latitude events; in these cases, plots like those in Figure 6 contain only symmetric clouds of points near the origin.

4. NITRIC OXIDE EMISSION AND ENERGY LOSS

Nitric oxide mid-wave IR (MWIR) emissions are a ubiquitous feature of the nighttime thermosphere, where they comprise the principal cooling mechanism below 200 km. Like those of carbon dioxide $4.3 \mu\text{m}$, they are greatly enhanced during aurora. One of the principal differences between these radiators is that the NO molecule is produced copiously in the auroral zone by reactions 8a and 8b. As a result, there is not only a lot of prompt emission directly resulting from the production of the entire manifold of vibrational states, but also an increase in total NO that emits following excitation by the quiescent airglow mechanism, the reverse of reaction 7. The additional population of NO is long-lived, and hence can be transported by strong winds blowing out of the auroral zone during geomagnetically disturbed conditions.

One of the purposes of the present paper is to illustrate how energy deposited in the auroral zone is redistributed and removed from the atmosphere by radiation at other locations. To do this most accurately would require us to distinguish emissions that represent true cooling of the atmosphere from those that merely reradiate deposited auroral energy before it is thermalized. [The difference is that in the case of cooling, excitation via the reverse of reaction 7 removes energy from the thermal bath prior to the emission at $5.3 \mu\text{m}$, whereas this does not happen when emitting states are directly

produced by the aurora.] However, this cannot be easily done without further modeling and assumptions and is beyond the scope of this paper.

We note that the 5.3- μm emission does represent energy loss, if not necessarily true cooling, and we will show how it varies between quiet times and storm conditions. Further discussion of these issues can be found in the recent work of *Mlynczak et al.*²² and in future publications.

SABER channel 6 measures NO(v) 5.3- μm emission in a bandpass that covers 1865-1945 cm^{-1} (5.36-5.14 μm) at the 5% transmission points. This bandpass was designed to preferentially detect emission from the NO(v=1) state, but it also includes emission from the 2-1 and 3-2 hot bands. For emissions that are characterized by a rotational temperature of 296K, about 60% of channel-6 radiance originates from the fundamental, 48% from the 2-1 band and 15% from the 3-2 band²². Because these fractions are sensitive functions of the widths of the rotational-line spectrum of each band, they will vary significantly with altitude in the thermosphere as the temperature rapidly increases with height.

To obtain the energy loss from NO, one must first obtain the total volume emission rate (VER) by inverting the limb radiance. The limb radiance from NO is optically thin, allowing the use of an Abel inversion^{23,24}. The inversion process yields a vertical profile of the VER, in units of $\text{W}/\text{cm}^2\text{-sr}$. To obtain the total 5.3- μm emission rate, however, we must know what fraction of the total radiance is contained in the channel-6 bandpass. A conversion factor,²² or "unfilter factor" $U(z)$, multiplies the emission in the bandpass to obtain the total emission. This factor depends upon the temperature and the relative contributions from reactions 7 and 8. It can be calculated, but not from SABER/TIMED data alone. A MSIS-90E reference atmosphere for high solar activity is used to provide input densities and temperatures. Then the NO vibrational temperature model of *Funke and Lopez-Puertas*¹⁶ is used to calculate $U(z)$, which varies from about 2.5 at 120km to 3.9 at 200km during storm conditions, and ultimately to compute the energy loss rate.

Figure 7 shows the volume energy loss rate averaged over a 5-degree latitude bin at 82S for April 15, prior to the major storm activity, and April 18 when the storm effects were very pronounced. The storm has increased the energy loss rate by about a factor of four. These loss rates are centered at fairly high altitudes. Note that when the loss rate is expressed in K/day, as in Figure 7, it is not simply proportional to the energy emitted per unit volume per unit time but is also inversely proportional to the density. For this reason, it peaks at a higher altitude than the emitted energy.

The processes that determine NO(v) populations and the corresponding emission are complex, but they have been discussed widely in the literature^{17,18}. Without either enough spectral resolution to measure the NO(v) distribution and thus infer its sources, or measurements of temperature and composition, these processes cannot be clearly delineated. However, the global behavior of the NO emitted energy during the storm period will make several points clear.

Figure 8 is a composite of the height-integrated energy loss over the southern hemisphere. Starting in the upper left on April 15, just around the time of the first increase of geomagnetic activity the flux of radiated energy is below $6 \times 10^{-4} \text{ W}/\text{m}^2$. There are slightly higher loss rates in the auroral zone (displaced from the geographic pole) and at near-equatorial latitudes. The darkest circle poleward of about 84S indicates where no data is available. In the projections that follow (left-to-right, then down) we see that April 17 and then April 18 show increases to greater than $2.3 \times 10^{-3} \text{ W}/\text{m}^2$ in the auroral zone, and on the peak day April 20 (day 110) loss rates of over 2.3×10^{-4} extend northwards over Australia to latitudes around 30 S. These are well beyond the zones of energy input seen in channel 7, channel 8 and GUVI. On April 21, when K_p has fallen abruptly, we see a rapid decrease in the amount and spatial extent of NO emitted energy, but not to the very low pre-storm levels.

Figure 9 compares the SABER channel 7 (at 120km tangent altitude) and channel-6 (at 130km tangent altitude) limb emission rates over the globe for April 19 near the peak of the storm and April 21 when the storm has decreased dramatically. Here we see again that channel-7 radiance, a proxy for auroral input as discussed above, is confined to the auroral zone, which is much expanded on the 19th compared to the 21st. The NO 5.3- μm emission on the 19th, however, extends equatorward as far south as 20N in the northern hemisphere and 25S in the southern hemisphere at strengths comparable to those in the auroral zone. On April 21, although both emissions are significantly reduced, the NO emissions continue to extend much further equatorward than the channel-7 emissions.

The simplest case to analyze is that for quiescent or low-latitude nighttime conditions. With no electron-impact excitation, reactions 8 play a minor role. Then the excitation of the radiating state is almost entirely due to collisions with atomic oxygen and the emissions result in true cooling of the atmosphere. One can see that during and immediately after the strongest storm days the NO emissions are greatly enhanced at lower latitudes where there is no sign of auroral

excitation in channels 7 or 8, or from GUVI. The increased radiance can come from two sources. These are (1) excess NO transported from the high latitudes, and possibly some produced *in situ* by X-rays from flares; and (2) an increase in the rate of reaction 8b caused by higher temperatures and/or greater O₂ densities also resulting from dynamical adjustment to the increased geomagnetic input (atmospheric heave). These emissions at lower latitudes remain visibly elevated two days past the peak of the storm, but in another day or two (not shown) they return to their original levels. The storm energy is thus absorbed, transported, and ultimately removed from the atmosphere on time scales of a few days.

At high latitudes in the auroral zone the NO emission and energy loss is maximum (see Figure 8) and the situation is more complicated. Reactions 8a and 8b contribute to the production of NO(v) as there is abundant production of N(⁴S) and N(²D) in the aurora. This source of NO(v) is in addition to the processes mentioned above that occur in lower latitudes. The N(²D) source is very short-lived after the source is turned off since its reaction lifetime with either O₂ or O is minutes or less. The N(⁴S) lifetime is longer, being determined by k_{8b} and by reaction 3 with NO to produce N₂ + O. This allows for some equatorward transport of N(⁴S) as well as of the longer-lived NO. However, mid-latitude decay of the high-altitude emission is not dramatically faster than that within the auroral zone. This indicates that even there the NO(v) concentration is not being dominated by production through reaction 8a. To determine the fraction produced through reaction 8a more accurately without spectral information is difficult. Analysis of the time behavior of channel-6 emission could provide some additional insight, but this is a complex task since successive orbits do not view the same regions and, even if one had information for earlier times, some knowledge of the winds would be necessary.

5. CONCLUSIONS

The 4.3- μ m and 5.3- μ m SABER channels respond dramatically to the geomagnetic storm conditions observed during April 2002. The 4.3- μ m channel nighttime limb radiance can approach a factor of 20 above the ambient values in the auroral zone. The geographical extent of its emission is very similar to that of the GUVI longer-wave LBH-2 band, and thus this channel responds, although imperfectly, to the auroral energy input. On a global geographical scale this correlation is consistent with our knowledge of the excitation processes for CO₂ v₃ and NO⁺(v). An unexpected result was the auroral enhancement in the 2.0- μ m channel that was designed to measure OH high vibrational levels. This channel-8 emission correlates well with the 4.3- μ m channel, but even better with the GUVI LBH-2, indicating that it is a prompt emission and suggesting that it might serve as a good auroral monitor within the SABER data set. Thus at nighttime SABER can detect auroral influence without other instruments as long as the aurora is strong enough to enhance channel 8 above the noise level. Further work is being done to identify the auroral emitter or emitters in channel 8.

The NO 5.3- μ m channel responds to geomagnetic storm input in a more complex manner. It is also highly enhanced during the storm periods, but this enhancement extends further equatorward than the expanded auroral oval determined by the channel-7, channel-8, and GUVI emissions. The NO(v) excitation process is a more complex mixture of V-T quiescent airglow processes and auroral chemiluminescence, but all emission represents energy loss from the thermosphere that is greatly enhanced during the active storm period. The fact that enhanced energy loss extends well equatorward into regions where there is no auroral input indicates that the storm energy-input response is global in nature. Since NO(v) is an effective cooling agent for the middle thermosphere, the heightened energy loss that we measure is a major reason the atmosphere relaxes back to its pre-storm values within a few days after the extra storm-time high latitude source is turned off.

ACKNOWLEDGEMENTS

We are grateful to Kent Miller of the Air Force Office of Scientific Research for support of this work. We also acknowledge the contributions of the other members of the NASA SABER Science Team.

REFERENCES

1. Yee, J.-H., G. E. Cameron, D. Y. Kusnierkiewicz, Overview of TIMED, *Proc. SPIE*, **3756**, 244, 1999
2. Russell, J.M. III, M.G. Mlynczak, L.L. Gordley, J. Tansock, and R. Esplin, An overview of the SABER experiment and preliminary calibration results, *Proce SPIE*, **3756**, 277-288, 1999.

3. Paxton, L.J., A.B. Christensen, D.C. Humm, B.S. Ogarzalek, C.T. Pardoe, D. Morrison, M.B. Weiss, W. Crain, P.H. Lew, D.J. Mabry, J.O. Goldsten, S.A. Gary, D.F. Persons, M.J. Harold, E.B. Alvarez, C.J. Ercol, D.J. Strickland, and C.-I. Meng, Global Ultraviolet Imager (GUVI): Measuring composition and energy inputs for the NASA Thermosphere Ionosphere Mesosphere Energetics and Dynamics (TIMED) mission, *Proc SPIE*, **3756**, 265-276, 1999.
4. Baker, K.D., D.J. Baker, J.C. Ulwick, and A.T. Stair, Jr., Measurements of 1.5- to 5.3- μm infrared enhancements associated with a bright auroral breakup, *J. Geophys. Res.*, **82**, 3518, 1977.
5. Kumer, J.B., Theory of the CO_2 4.3 μm aurora and related phenomena, *J. Geophys. Res.*, **82**, 2203, 1977.
6. Whalen, J. A., R. R. O'Neil, and R. H. Picard, The aurora, in Handbook of Geophysics and the Space Environment, A. S. Jursa, ed., Air Force Geophysics Laboratory, Bedford, Mass, U.S.A., pp1201-12-42, 1985.
7. Winick, J.R., R.H. Picard, R.A. Joseph, R.D. Sharma, and P.P. Wintersteiner, An infrared spectral radiance code for the auroral thermosphere (AARC), ADA202432, Air Force Geophysics Laboratory, Hanscom AFB, Mass., 1987.
8. Nebel, H., P.P. Wintersteiner, R.H. Picard, J.R. Winick, and R.D. Sharma, CO_2 non-LTE radiative excitation and infrared dayglow at 4.3- μm : Application to SPIRE data, *J. Geophys. Res.* **99**, 10409-10419, 1994.
9. Lopez-Puertas, M., and F.W. Taylor, Carbon dioxide 4.3- μm emission in the Earth's atmosphere: A comparison between NIMBUS 7 SAMS measurements and non-LTE radiative transfer calculations, *J. Geophys. Res.*, **94**, 13045-13068, 1989.
10. Lopez-Puertas, M., G. Zaragoza, M.A. Lopez-Valverde, and F.W. Taylor, Non local thermodynamic equilibrium (LTE) atmospheric limb emission at 4.6 μm 1. An update of the CO_2 non-LTE radiative transfer model, *J. Geophys. Res.*, **103**, 8499-8513, 1998.
11. Winick, J.R., R.H. Picard, R.D. Sharma, R.A. Joseph, and P.P. Wintersteiner, Radiative transfer effects on aurora enhanced 4.3 μm emission, *Adv. Space Res.* **7** (no.10) 17, 1987.
12. Smith, M.A., V.M. Bierbaum, and S.R. Leone, Infrared chemiluminescence from vibrationally excited NO^+ : product branching in the $\text{N}^+ + \text{O}_2$ ion-molecule reaction, *Chem. Phys. Lett.*, **94**, 398-403, 1984.
13. Hwang, E.S., K.J. Castle, and J.A. Dodd, Vibrational relaxation of $\text{NO}(v = 1)$ by oxygen atoms between 295 and 825 K, *J. Geophys. Res.*, **108**(A3), 1109, doi:10.1029/2002JA009688, 2003.
14. Caledonia, G.E. and J.P. Kennealy, NO infrared radiation in the upper atmosphere, *Planetary Space Sci.*, **30**, 1043-1056, 1982.
15. Kockarts, G. Nitric oxide cooling in the terrestrial thermosphere, *Geophys. Res. Lett.*, **7**, 137-140, 1980.
16. Funke, B. and M. Lopez-Puertas, Nonlocal thermodynamic equilibrium vibrational, rotational, and spin state distribution of $\text{NO}(v=0, 1, 2)$ under quiescent atmospheric conditions, *J. Geophys. Res.*, **105**, 4409-4426, 2000.
17. Dothe, H., J.W. Duff, R.D. Sharma, and N.B. Wheeler, A model of odd nitrogen in the aurorally dosed nighttime terrestrial thermosphere, *J. Geophys. Res.*, **107**(A6), 1071, doi:10.1029/2001JA000143, 2002.
18. Sharma, R.D., H. Dothe, and J.W. Duff, Model of the 5.3 μm radiance from NO during the sunlit terrestrial thermosphere, *J. Geophys. Res.*, **103**, 14753-14758, 1998.
19. Sharma, R.D., and J.W. Duff, Determination of the translational temperature of the high altitude terrestrial thermosphere from the rotational distribution of the 5.3 μm emission from $\text{NO}(v=1)$, *Geophys. Res. Lett.*, **24**, 19, 2407-2410, 1997.
20. Ajello, J.M., and D.E. Shemansky, A reexamination of important N_2 cross sections by electron impact with application to the dayglow: The Lyman-Birge-Hopfield band system and $\text{NI}(119.99\text{nm})$, *J. Geophys. Res.*, **90**, 9845-9861, 1985.

21. Cartwright, D. C., Vibrational populations of excited states of N₂ under auroral conditions, *J. Geophys. Res.*, **83**, 517-531, 1978.
22. Mlynczak, M.G., F.-J. Martin-Torres, J. Russell, K. Beaumont, S. Jacobson, J. Kozyra, M. Lopez-Puertas, B. Funke, C.J. Mertens, L. Gordley, R. Picard, J. Winick, P. Wintersteiner, and L. Paxton, The natural thermostat of nitric oxide emission at 5.3 μm in the thermosphere observed during the solar storms of April 2002, accepted for publication by *Geophys. Res. Lett.*, **30**, 2003.
23. Hays, P.B. , and R.G. Roble, Stellar occultation measurements of molecular oxygen in the lower thermosphere, *Planet. Space Sci.*, **3**, 339-348, 1973.
24. Zachor, A., R.D. Sharma, R.M. Nadile, and A.T. Stair Jr., Inversion of SPIRE NO data, *J. Geophys. Res.*, **90**, 9776-9782, 1985.

SABER FOCAL PLANE ARRAY

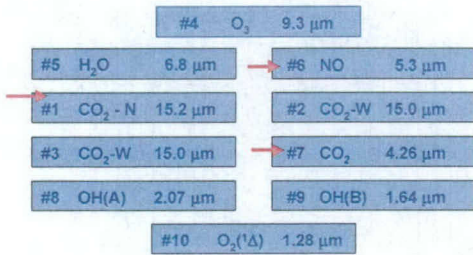


Figure 1. SABER focal plane array, listing the centers of the bandpasses and principal emitters for each channel.

CO₂ 4.3 μm Radiance at 110 km Tangent Height

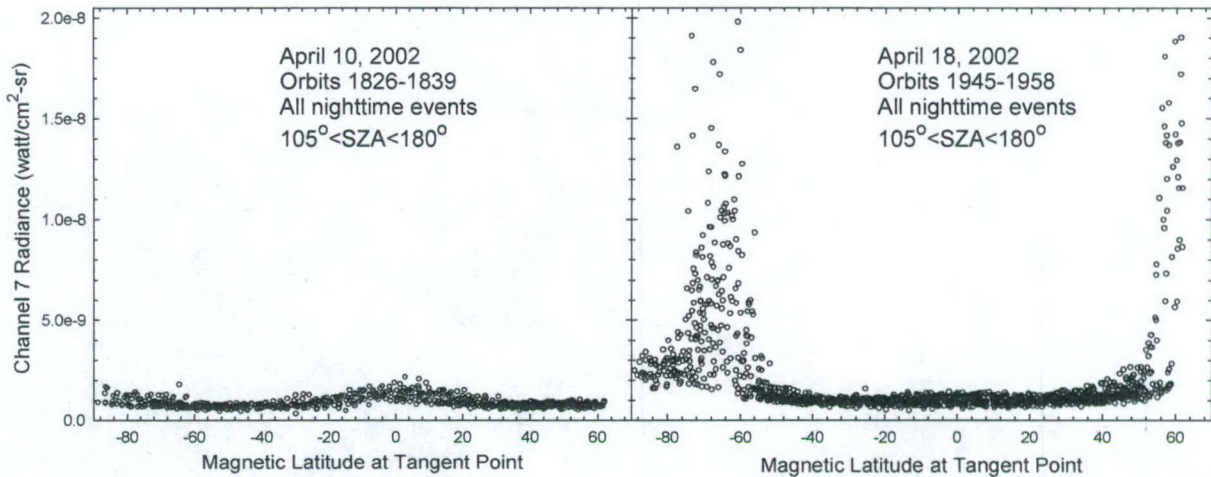


Figure 3. SABER channel 7 radiances at a tangent height of 110 km, as a function of magnetic latitude for a quiet day (April 10) and a storm day (April 18). The enhanced emissions and expanded auroral zone are clearly evident for disturbed conditions.

SABER Limb Radiance, April 18, 2002

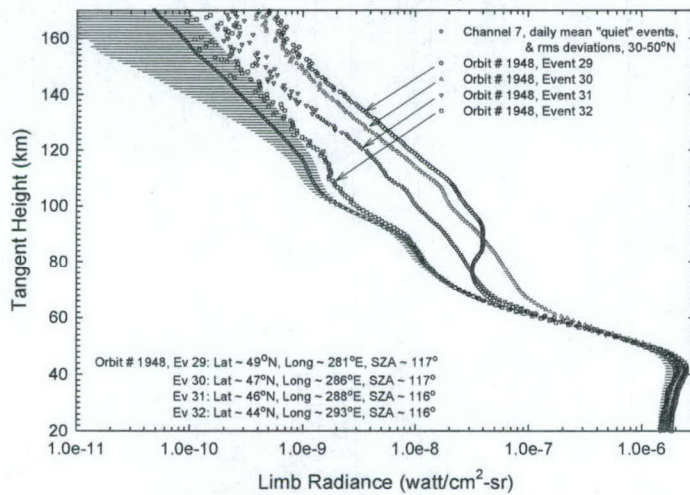


Figure 4. SABER individual and composite radiance profiles for a storm day, April 18. The average "quiet" profile, shown with the associated rms deviations, was constructed from all events between 30 and 50°N latitude revealing no sign of auroral dosing. Four individual auroral events illustrate event-to-event variability in the extended auroral zone.

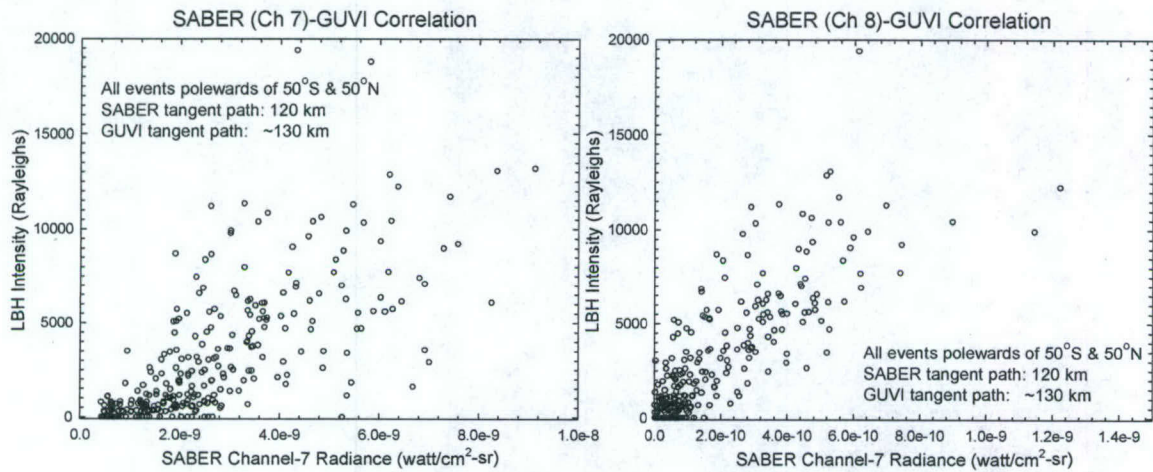


Figure 6. Correlation between SABER and GUVI limb radiance, for all events polewards of 50° magnetic latitude on a storm day, April 18. SABER data are given for channels 7 (4.3 μm) and 8 (2.0 μm).

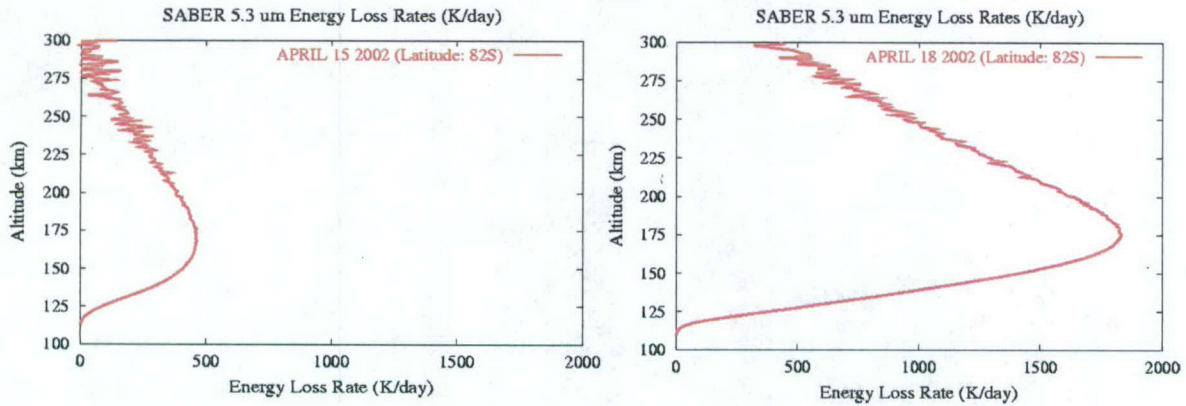


Figure 7. Total energy loss rate from 5.3-μm emission, for typical SABER events at high latitude, on a quiet day (April 15) and a storm day (April 18).

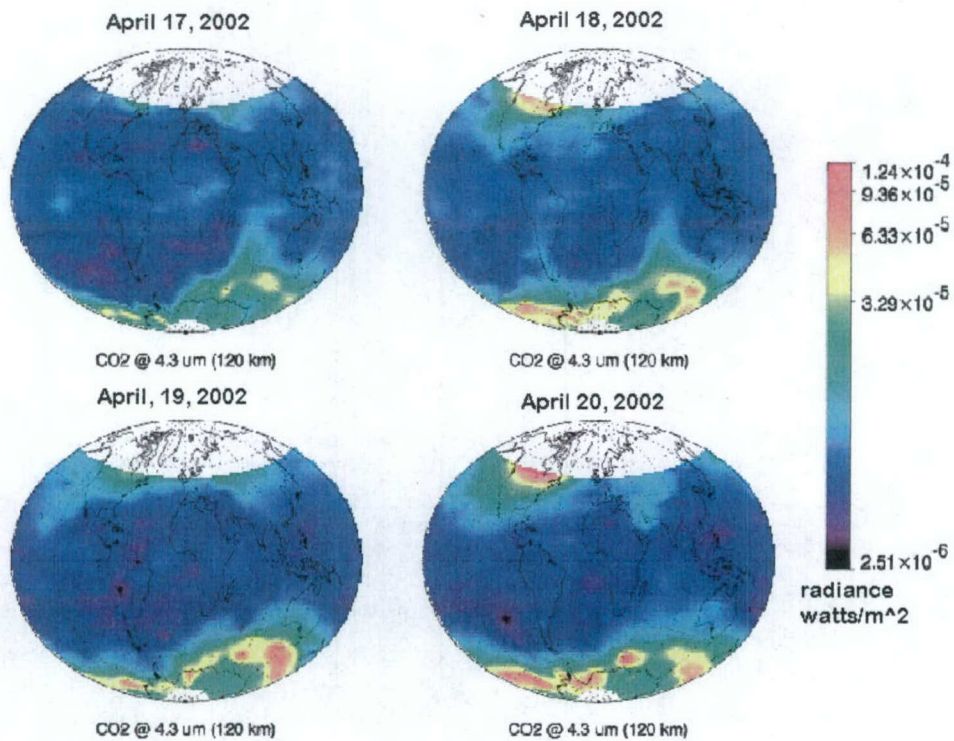


Figure 2. Global limb radiance maps from SABER channel 7 at tangent height of 120km, for four days preceding and during the main phase of the April geomagnetic storm

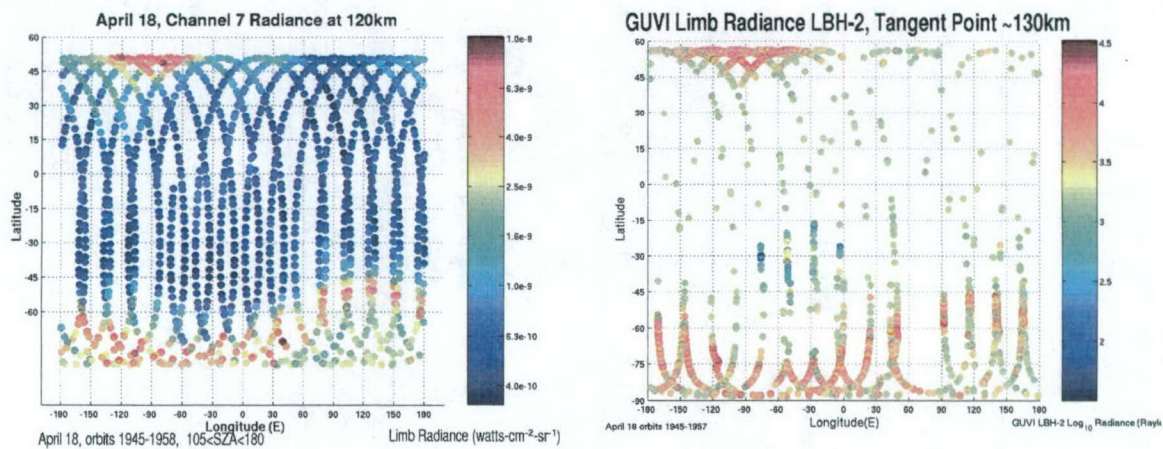


Figure 5. Global morphology of CO₂ 4.3 μm and LBH-2 limb radiance for tangent heights in the lower thermosphere for a storm day, April 18. Units of GUVI radiance are Rayleighs (logarithmic color scale).

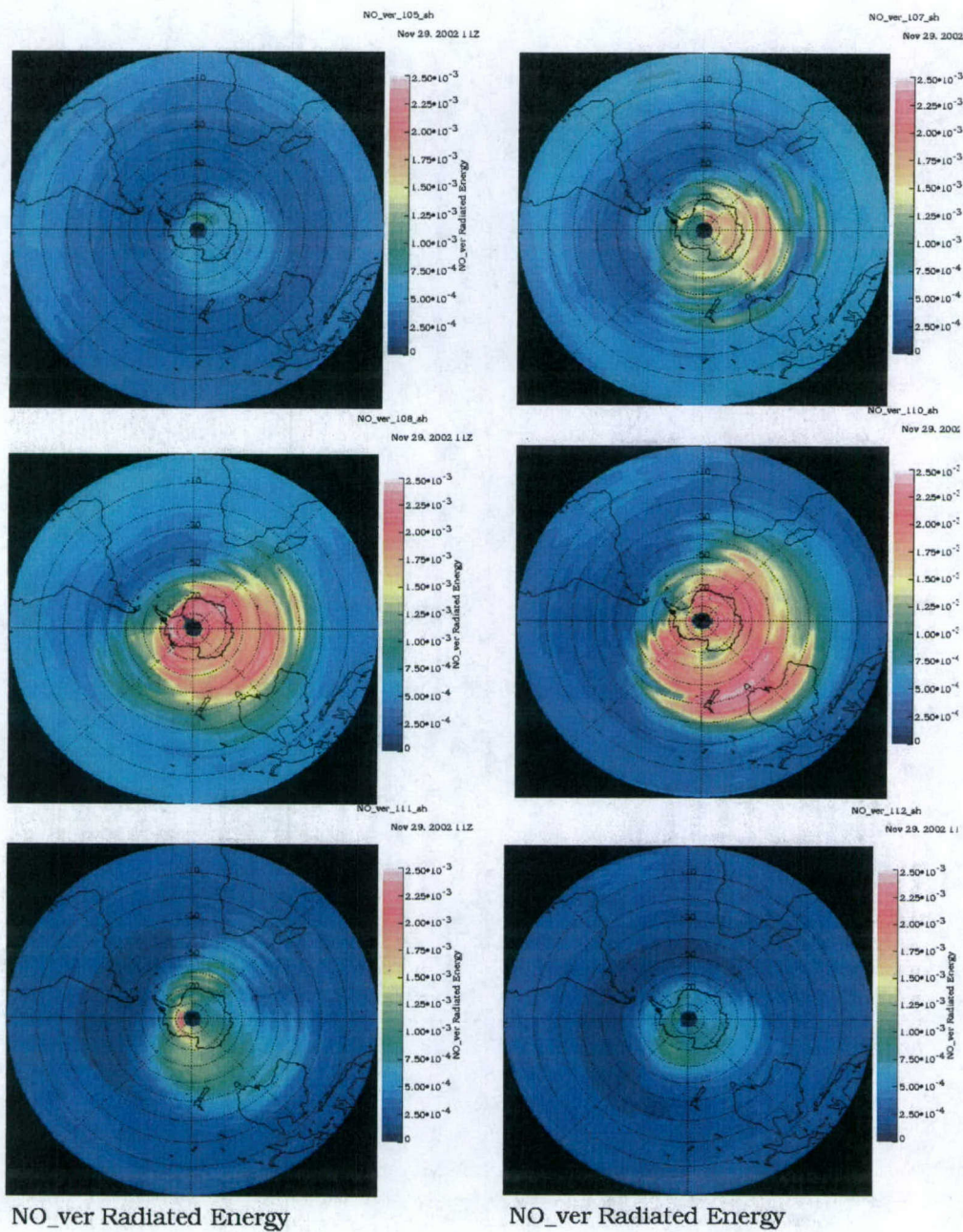


Figure 8. Flux of energy radiated at 5.3 μm in the southern hemisphere, for six days before, during, and after the April 2002 geomagnetic storm period. Panels show data for April 15 (top left), April 17 (top right), April 18 (middle left), April 20 (middle right), April 21 (bottom left), and April 22 (bottom right). Data range from 0 to $2.5 \times 10^{-3} \text{ W/m}^2$.

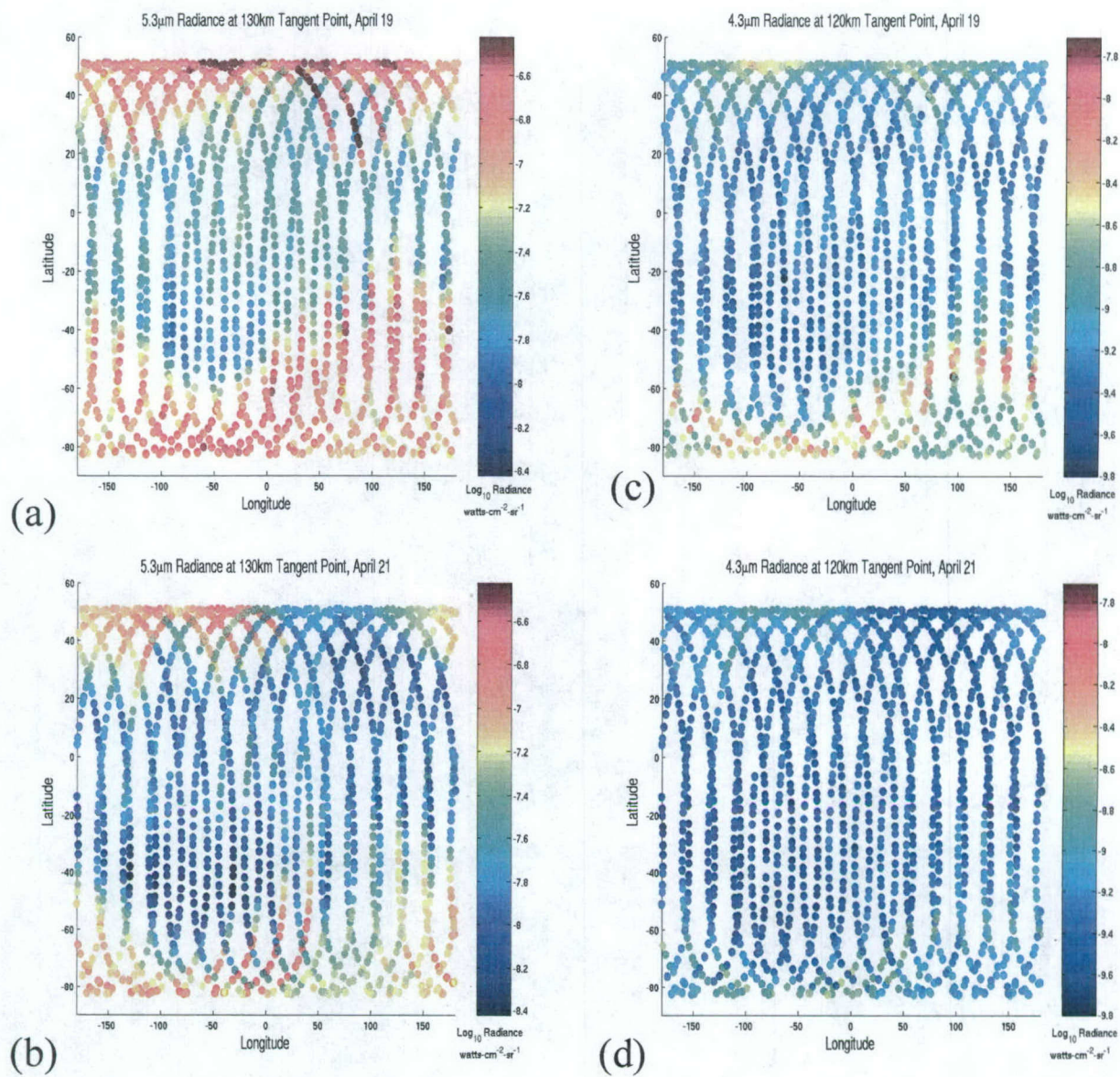


Figure 9. Global maps of NO and CO₂ limb radiance for April 19 (panels a & c) and April 21 (b & d). The storm was near its peak on the 19th and greatly diminished by the 21st. By the 19th, NO densities outside the auroral zone were already greatly enhanced by transport. The residual effects are still clearly seen in NO emission on the 21th (panel b), even though dosing levels were quite low (as implied by panel d). Radiance values in W/(cm²-sr) are plotted on a log scale NO values range from